Interfacial Assembling of Flexible Silica Membranes with High Chlorine Resistance for Dye Separation

Guodong Kong, Ge Yang, Panpan Xu, Zixi Kang, Hailing Guo, Mengling Sun, Zifeng Yan, Svetlana Mintova, Daofeng Sun

Interfacial Assembling of Flexible Silica Membranes with High Chlorine Resistance for Dye Separation

Guodong Kong[a], Ge Yang[a], Panpan Xu[a], Zixi Kang[b]*, Hailing Guo[a]*, Mengling Sun[a], Zifeng Yan[a], Svetlana Mintova [a,c], Daofeng Sun[b]

[a] State Key Laboratory of Heavy Oil Processing, Key Laboratory of Catalysis, China National Petroleum Corp. (CNPC), China University of Petroleum (East China), Qingdao, Shandong, 266580, PR China.

[b] School of Materials Science and Engineering, China University of Petroleum (East China), Qingdao, Shandong, 266580, PR China

[c] Normandie Universite, ENSICAEN, UNICAEN, CNRS, Laboratoire Catalyse et Spectrochimie (LCS), 14050 Caen, France

* Corresponding authors.

E-mail addresses: guohl@upc.edu.cn (Hailing Guo); kzx@upc.edu.cn (Zixi Kang)

Abstract

Inorganic membranes have gained extensive attention due to their more uniform pore size, higher flux, and better chemical stability over traditional polymeric membranes. However, the development of inorganic membranes still faces substantial obstacles in the form of a difficult preparation procedure and the high cost of a large-scale synthesis. Herein, a facile interfacial assembly strategy is designed to prepare flexible silica membranes by the close and strong packing of ultra-small nanoparticles via crosslinking with trimesoyl chloride. Profiting from the extremely small size and tight packing of silica nanoparticles, the permeance of flexible silica membrane with a uniform pore size of 3.4 nm exceeds 210 L m^{-2} h^{-1} MPa^{-1}, which is nearly 11 times higher than the polyamide membrane simultaneously ensuring the rejection effect. Meanwhile, the flexible silica membrane has no performance deterioration after exposure to 50000 ppm h of chlorine (NaOCl), indicating its excellent chlorine resistance. The facile interfacial assembly strategy applied for the synthesis of the membrane is highly reproducible and scalable (high-performance silica membrane with 100 cm^2 has been obtained), which has overall flexibility after the curvature of 100 m^{-1}, paving the way for the development of future applications.

Keywords: Silica Nanoparticles; Interfacial assembly; Nanofiltration; Chlorine Resistance.

1. Introduction

Water contamination and shortage have evolved to be a global issue due to rapid population and economic growth. Increasing water supply by desalination of seawater and recycling wastewater are crucial for alleviating global water scarcity[1]. Nowadays, one of the primary contributors to the current water contamination is wastewater from the textile and dyeing industries[2-5]. The separation of dyes by traditional methods such as distillation, adsorption, and extraction often imposes the heaviest economic burden and the largest environmental footprint[6-9]. Fortunately, the energy consumption during these separation processes can be drastically decreased by using high-performance membranes instead of the phase change process [10-12].

Currently, polymeric membranes are the most widely applied commercial membranes for water treatment due to their ease of processing, and low cost [1, 13]. Thin-film composite (TFC) membranes prepared by interfacial polymerization (IP) dominate the commercial market[14]. In the IP process, amine monomers diffuse from an aqueous solution into an organic solvent phase, reacting with acyl chlorides at the two-phase interface and generating a highly cross-linked polyamide network[15, 16]. However, the active layer based on the amide linkage is generally susceptible to chlorine attacks resulting in N-chloro derivatives[17]. Such reactions damage membrane integrity, leading to performance loss and hindering membrane lifetime. Besides, it has proven difficult to prepare a membrane with a permanent interconnected free volume and a narrow aperture-size distribution in a process far from thermodynamic equilibrium[15]. Therefore, it becomes challenging to overcome the trade-off restrictions between permeability and selectivity for TFC membranes[18, 19]. Consequently, it is extremely urgent to find new membrane materials with high flux and rejection while achieving high chlorine resistance.

In contrast, inorganic membranes are competitive candidates for separation membranes due to their well-defined pore size, stronger chemical stability, and more extended membrane longevity[20-22]. However, the cost and energy consumption for the preparation process of metal oxide membranes is too large, which is not conducive

to large-scale production and practical application[23]. Especially, metal oxide membranes including Al_2O_3 and TiO_2 require high sintering temperatures (1000 ^oC) and energy input, which are crucial for ceramic densification[24]. For example, in the process of fabricating γ-alumina ceramic membrane by coating boehmite sols followed by heat treatment, defects are inevitably formed resulting in a sharp decrease in the selectivity of the membrane and a significant reduction in the lifetime[25]. Taking another example, zeolite and MOF membranes were usually obtained by hydrothermal or solvothermal synthesis at a laboratory scale[26-28]. *In-situ* growth has proven to be a demanding task due to the substrate's poor heterogeneous nucleation site of MOF. Increasing substrate nucleation site density through pre-seeding and substrate modification was suggested, while these additional procedures complicate the synthesis process[29, 30]. Overall, the high cost and complex preparation process of these inorganic membranes remain significant obstacles to their commercialization process[23].

Herein, the IP process, which has been highly recognized in TFC membranes, was adopted to prepare inorganic membranes. As shown in **Scheme 1**, we selected the ultra-small sized silica nanoparticles as the water monomer, and highly reactive TMC as the oil monomer, then a continuous and dense flexible silica membrane is obtained on the polyethersulfone (PES) substrate through a two-phase crosslinking reaction. Compared to inorganic membranes or TFC membranes described in the literature, the flexible silica membrane has the following advantages: Firstly, the interfacial assembly method and commercial polymer substrates bring ease of processing and potential for scale-up fabrication to the inorganic membrane. Second, a narrow pore size distribution is furnished to the membrane by tightly packed and strongly cross-linked silica nanoparticles for effective dye rejection. Thirdly, covalently cross-linked silica membranes possessed greatly improved chlorine resistance.

2. Experiments

2.1. Materials

Methyl blue ($C_{37}H_{27}N_3Na_2O_9S_3$, 98%), methyl orange ($C_{14}H_{14}N_3SO_3Na$, 99%), Congo red ($C_{32}H_{22}N_6Na_2O_6S_2$, 99%), sodium chloride (NaCl, 99%), sodium sulfate (Na_2SO_4,

99%), magnesium chloride ($MgCl_2$, 99%), M-phenylenediamine (MPD, $C_4H_{10}N_2$, > 99%) and sodium hypochlorite aqueous solution (NaOCI, 7 - 8%) were bought from Sinopharm Chemical Reagent Co., Ltd., China. PES membrane (GC-UF0202) as the substrate for TFC and flexible silica membranes was bought from Guochu Technology (Xiamen) Co., Ltd. Trimesoyl chloride (TMC, > 99.0%) and Colloidal silica (LUDOX® HS-30) were bought from Sigma-Aldrich. Cyclohexane (C_6H_{12}, 99.5 %) was bought from Tian Jin Fuyu Fine Chemical Co., Ltd. The poly(ethylene glycol)s (PEGs, MW = 2000, 4000, 6000, 8000, 10000) were bought from Maclin Chemical Reagent Co., Ltd.

2.2 Fabrication of PA TFC membrane

The PES support was cleaned by immersing it in DI water for 12 hours. Firstly, 10 mL of MPD aqueous solution (1 %) was spread onto the PES support. The MPD aqueous solution on the support was removed by an air knife after impregnating for 5 mins. Then, 10 mL of TMC in cyclohexane solution (0.1 %) was spread onto the PES substrate and reacted for 1.5 mins. After the reaction is complete, the oil phase is poured out and the surface of the membrane is rinsed with cyclohexane. Eventually, the PA TFC membrane was baked for 5 minutes at 333 K. The obtained PA TFC membrane is named **M-PA**.

2.3 Fabrication of flexible silica membrane

The flexible silica membranes were prepared by an *in-situ* interfacial assembly method (**Scheme 1**). Firstly, 1 wt.% SiO_2 solution was prepared by diluting 1 mL of colloidal silica (30 wt.% in H_2O) with 30 mL DI water followed by ultrasonic treatment for 1 min. Then, the PES substrate was placed horizontally on a holder inside the homemade container. Subsequently, 30 mL of SiO_2 dispersions was poured into the container until it exceeded the surface of the substrate. Then, 10 mL of a TMC (0.2 %) in organic (cyclohexane) solution was poured slowly onto the SiO_2 dispersion. After 2.5 - 10 mins (**Table 1**), the outlet at the bottom of the container is opened. As the solution flows out from the bottom of the container, the synthesized membrane slowly falls on the substrate surface of the PES. Ultimately, the prepared membrane was placed in an oven at 333 K for 5 mins. These membranes are named **M-2.5**, **M-5**, and **M-10** respectively in accordance with the reaction time. The

preparation conditions of the enlarged membrane were consistent with **M-2.5**. The difference is the use of a larger PES substrate and mold.

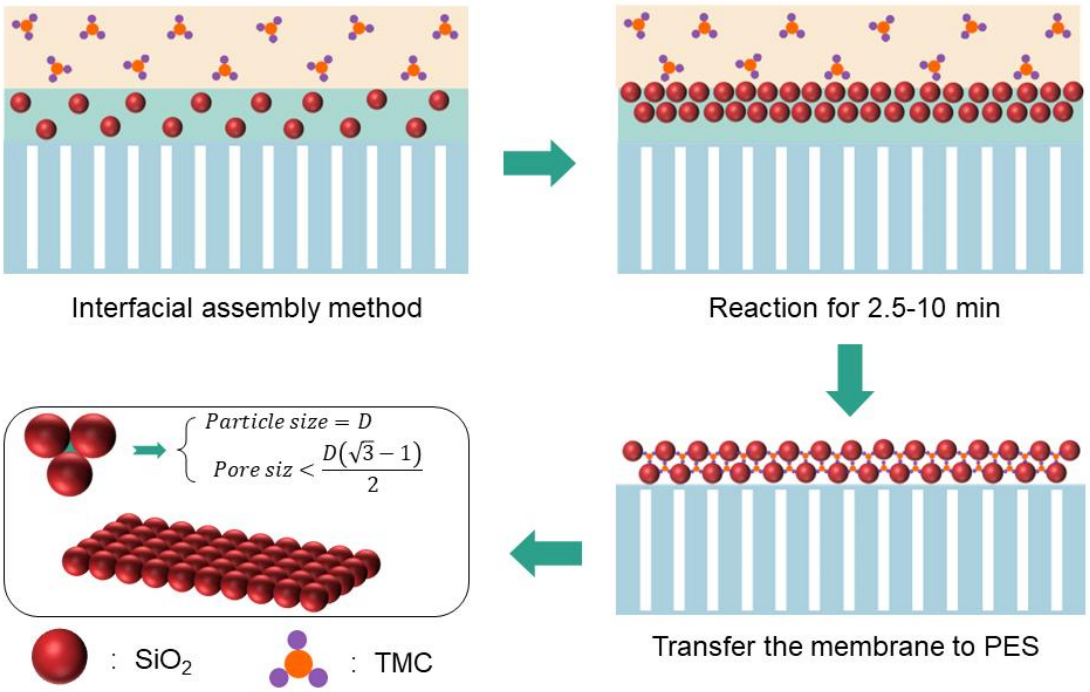

Scheme 1. The process of preparing flexible silica membranes through the interfacial assembly method.

Table 1. Summary of the preparation conditions for different membranes.

Membrane	MPD (m/V)	SiO_2 (m/V)	TMC (m/V)	IP duration (min)
PA(**M-PA**)	1%	-	0.1%	1.5
silica membrane (**M-2.5**)	-	1%	0.2%	2.5
silica membrane (**M-5**)	-	1%	0.2%	5
silica membrane (**M-10**)	-	1%	0.2%	10

2.4 Characterization

The structures of the amorphous SiO_2 nanoparticles were measured by X-ray diffraction (XRD, Ultima, XRD-6000, Japan) at the range of 5 - 65°. The particle size of the silica particles was analyzed by a nanoparticle analyzer (SZ-100Z, HORIBA, Japan) at 25 ^{o}C. The surface chemical functionality of membranes as prepared was examined using Fourier transform infrared spectroscopy (FTIR) spectra (Bruker Vertex 70V). The thermal stability of SiO_2 and flexible silica membranes are tested with TG-DTA (NETZSCH SAT449 F5) under an air atmosphere. The surface

morphology of membranes was tested with atomic force microscopy (SHIMADZU, SMP-9700) in tapping mode. At a 200 kV acceleration voltage, TEM images of membrane morphology and SiO_2 particle size were captured using an FEI Tecnai G20 transmission electron microscope. A nanoparticle analyzer (SZ-100Z, HORIBA, Japan) was taken to test the zeta potential values of SiO_2. The pore size distribution of the silica nanoparticles and flexible silica membranes were calculated according to the N_2 adsorption isotherms (Micromeritics ASAP 2020). The concentration of the filtrated water and feed solution was measured by a TOC analyzer (Shimadzu TOC-LCPH/CPN, Japan), and the rejection of the PEG was estimated according to that data. The concentration of organic dyes was assessed using the ultraviolet-visible (UV-vis) spectrometer (UV-2450, SHIMADZU, Japan). The conductivity meter (DDS -307, YUEPING, Shanghai) was used to test the concentration of the salt solution. The surface wettability of membranes was investigated using a contact angle goniometer (JC2000D). An electrokinetic analyzer (SurPASS, Anton Paar, Austria) was used to measure the surface charge properties of flexible silica membranes at various pH settings.

2.5 Evaluation of the pore size of the flexible silica membrane

The pore size of the flexible silica membrane was calculated by testing the rejection of PEGs with different molecular weights. The Stokes radius d_p (nm) of PEG was estimated according to Eq. (1):

$$d_s = 33.46 \times 10^{-3} \times M^{0.557} \quad (1)$$

where *M* is PEG molecular weight.

The pore size distribution of membrane can be estimated through the probability density function[31, 32], as shown in Eq. (2):

$$\frac{df(d_p)}{dd_p} = \frac{1}{d_p \ln \mathfrak{6}_p \sqrt{2\pi}} exp\left[-\frac{(\ln d_p - \ln \mu_p)^2}{2(\ln \mathfrak{6}_p)^2}\right] \quad (2)$$

Where d_p denotes the pore size of membranes. The pore size (μ_p) was equal to μ_s, which is the value corresponding to a solute with a Stokes diameter of 50% rejection. The geometrical standard deviation of the membrane ($\mathfrak{6}_p$) was equal to $\mathfrak{6}_s$, which is

a ratio between the Stokes radius with a rejection of 84.13% to that with a rejection of 50%.

2.6 Evaluation of membrane separation performance

The separation capabilities were assessed using a dead-end unit with an effective membrane area of 1.77 cm^2 under 0.2 MPa. The NF performance of the membranes was tested using 50 mL of methyl blue (MB), methyl orange (MO), and Congo red (CR) solution at a concentration of 50 ppm. The separation performance of the membrane was also tested by inorganic salts (Na_2SO_4, $MgCl_2$, NaCl) and PEGs. The concentrations of salts and PEGs solutions were 1000 ppm and 100 ppm, respectively. The standard deviation was calculated using the average results of two measurements. The water permeance J (L m^{-2} h^{-1} MPa^{-1}) was determined by the Eq. (3):

$$J = \frac{V}{A \times \Delta t \times \Delta P} \quad (3)$$

Where V (L) is the permeated water of dye or salt solution, A (m^2) is the effective filtration area, Δt (h) is the operation time, and ΔP (MPa) is the applied trans-membrane pressure. The pure water flux F (L m^{-2} h^{-1}) was determined by Eq. (4):

$$F = \frac{V}{A \times \Delta t} \quad (4)$$

The solute rejection (R) is determined by the Eq. (5):

$$\mathrm{R} = \left(1 - \frac{C_P}{C_f}\right) \times 100\% \quad (5)$$

Where C_p is the solute concentrations of the solution after permeation, C_f represents the concentrations of the feed solution.

2.7 Chlorine-resistance test of membranes

Chlorine resistance was detected by the static method. In brief, a membrane sample was immersed in NaOCl solution initially. During the chlorination process, the concentration of the NaOCl solution was maintained at 200 ppm. To avoid the decomposition of active chlorine, the NaOCl solution was also stored in the dark. The NaOCl solution was renovated every 72 hours to maintain a stable concentration of active chlorine. At intervals of 5 hours, took out the membrane sample from the solution and washed it with DI water three times, then placed it into a dead-end unit. Finally, the device was operated with 50 mL dye solution under 0.2 MPa.

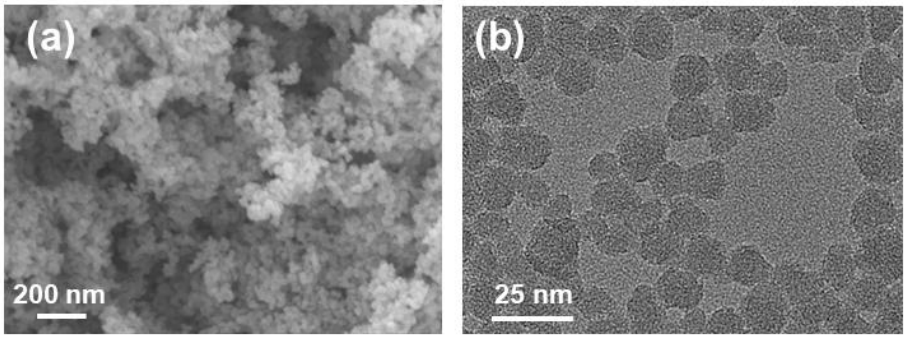

Fig. 1 (a) SEM and (b) TEM picture of SiO_2.

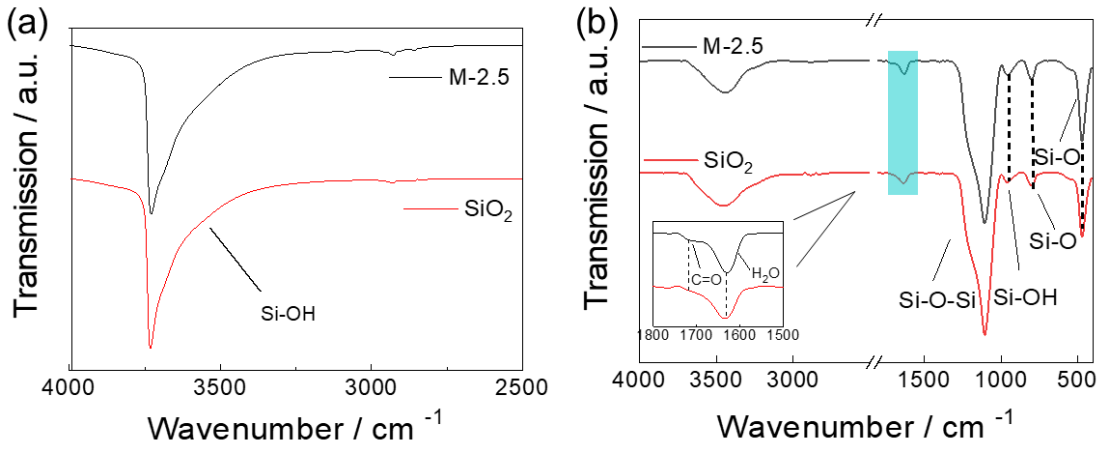

Fig. 2 (a) FTIR spectra of SiO_2 nanoparticles and **M-2.5** at 673 K; (b) FTIR spectra for SiO_2 nanoparticles and **M-2.5** at room temperature.

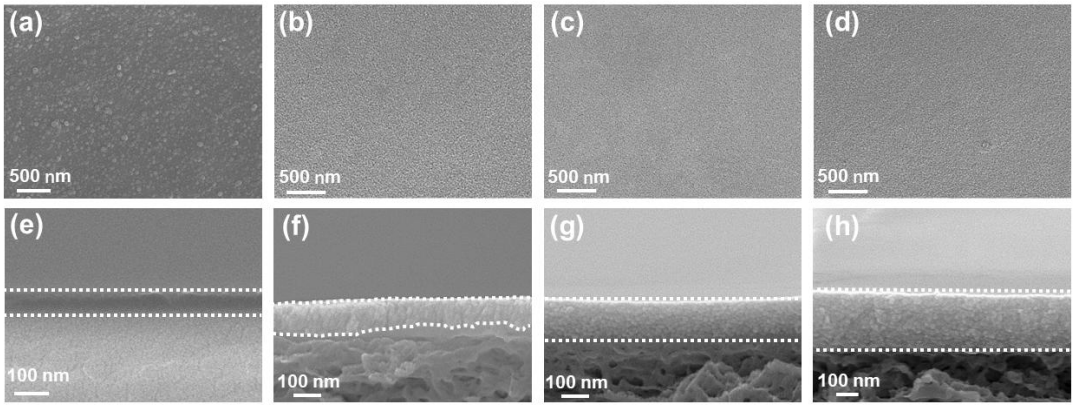

Fig. 3 The top-view SEM images of **M-PA** (a), **M-2.5** (b), **M-5** (c), and **M-10** (d); the cross-section SEM images of **M-PA** (e), **M-2.5** (f), **M-5** (g), and **M-10** (h).

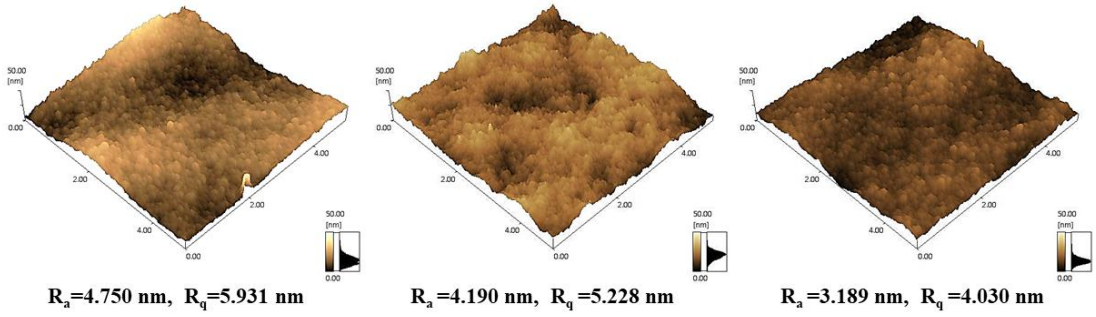

Fig. 4 AFM images and roughness of (a) **M-2.5**, (b) **M-5**, (c) **M-10**.

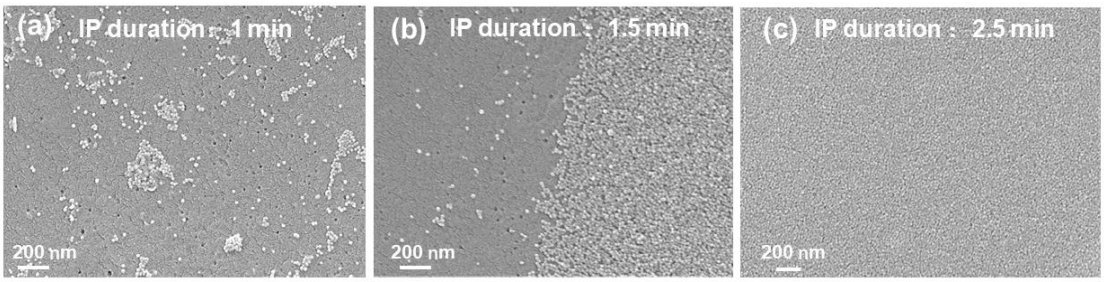

Fig. 5 SEM image for the flexible silica membrane with interfacial assembly times of 1, 1.5, and 2.5 mins respectively.

3. Results and discussion

3.1 Characterization of SiO_2 nanoparticles

As shown in **Fig. S1**, the XRD pattern shows a high-intensity and wide diffraction peak around the diffraction angle 2θ = 24°, indicating that the silica nanoparticles are amorphous. Observed from the SEM and TEM images in **Fig. 1**, the spherical SiO_2 nanoparticles have good dispersibility and uniform size (about 20 nm). The particle size distribution for SiO_2 deduced by the nanoparticle analyzer shows that the average particle size of the SiO_2 is around 18.5 nm (**Fig. S2**), which is in accordance with the results obtained from the TEM image. The ultra-small particle size of silica is one of the key factors to achieve tight interfacial assembly of continuous membranes. The zeta potential of the suspension containing SiO_2 was measured. The results (**Fig. S3**) showed that the zeta potential values of the silica nanoparticles were -25.2, -32.6, and -39.1 mV at pH = 4, 7, and 9, respectively, due to the presence of abundant silanol group (Si-OH, **Fig. 2**). More importantly, Si-OH can also act as a functional group, providing reactive sites for the interfacial assembly of silica nanoparticles with TMC.

3.2 The composition and morphology of flexible silica membrane

The FTIR was applied to characterize the silanol group at 673 K to avoid the effects of adsorbed water in SiO_2 nanoparticles. From **Fig. 2a**, it can be seen that the **M-2.5**

and pure SiO_2 have similar main absorption peaks at wavenumbers of 3730 cm^{-1} which are assigned to the silanol stretching vibration[33]. Silica and **M-2.5** were also characterized by FTIR at room temperature to demonstrate crosslinking between SiO_2 and TMC. To avoid the effect of free TMC hydrolysis on the absorption peak, the prepared **M-2.5** was washed sequentially with cyclohexane, ethanol, and water twice respectively. Finally, **M-2.5** was dried at 373 K for 2 hours for infrared characterization. As shown in **Fig. 2b**, the flexible silica membrane exhibits a weak stretching vibration peak at 1720 cm^{-1}, which confirms the formation of the ester bond and the crosslinking between the TMC and SiO_2 nanoparticles[34]. What's more, **Fig. 2b** shows that the strong absorption peak located at 1109 cm^{-1} corresponds to the asymmetric vibration of Si-O-Si, and the absorption peak located at 812 cm^{-1} and 476 cm^{-1} corresponds to the stretching and the bending vibration of Si-O respectively in **M-2.5** sample. It confirmed that the silica crosslinked by TMC tightly constitutes the main structure of the membrane.

Thermogravimetric tests were performed on **M-2.5** and SiO_2 nanoparticles to further characterize the ratio of silica to TMC in the flexible silica membrane (**Fig. S4**). For the flexible silica membrane, two weight-loss platforms are shown. The first platform is from room temperature to ~140 °C, which could be attributed to the evaporation of absorbed water molecules. The weight loss in the second stage ranging from 140 to 800 °C is 4.78 %, which is higher than that of pure SiO_2 nanoparticles (~1.95 %). It indicates that TMC accounts for ~2.83 % of the total mass in the flexible silica membrane. This result suggests that the silica nanoparticles act as the main building blocks of the membrane with the assistance of the TMC crosslinkers.

The surface features of the flexible silica membrane were characterized with SEM (**Fig. 3**) and AFM (**Fig. 4**). The flexible silica membrane exhibits a uniform and smooth surface topography without obvious void defects. It indicates that the interfacial assembly method can quickly realize the uniform and ordered arrangement of silica nanoparticles, which is of great importance for the scale-up preparation of inorganic membranes. The cross-sectional SEM images show that the flexible silica membranes are composed of tightly packed silica nanoparticles (**Fig. 3f-h**). In addition, the **M-2.5** has a minimum thickness of about 100 nm. With the extension of reaction time, the thickness of the flexible silica membranes increases from ~100 nm (**M-2.5**) to ~240 nm (**M-10**). The silica nanoparticles on the PES substrate are

distributed uniformly throughout the flexible silica membranes according to the EDS mapping results (**Fig. S5**). The surface topography and roughness of the membrane were also detected by AFM (**Fig. 4**). **M-2.5** has the highest surface roughness, and the average roughness decreases gradually as the reaction time increases. With the prolongation of the reaction time, the TMC monomer needs to diffuse through the nascent membrane to further assemble. Therefore, the TMC monomer diffusion rate is faster in regions with more voids, which means the assembling rate of SiO_2 nanoparticles is relatively higher. Therefore, as the reaction progresses, the membrane surface becomes more uniform and smoother.

To further explore the assembly process of flexible silica membranes, the morphologies of the membrane surfaces after different reaction times were observed and compared in the SEM images. **Fig.5a** shows that silica nanoparticles reacting with acid chloride monomers form primary clusters or aggregates in a disordered distribution state at a reaction time of 1 min. As the reaction progresses, the silica spheres connect to form a nascent membrane that continues to assemble along the edges of the membrane **(Fig. 5b)**. When the reaction time is further prolonged, the stacking of silica nanoparticles became more compact with the assistance of TMC **(Fig. 5c)**. Besides, the degree of dispersion of the particles determines whether a continuous dense surface structure can be synthesized. As shown in **Fig. S6a**, the membrane prepared using uniform dispersed silica nanoparticles has a uniformly smooth and defect-free membrane surface. In contrast, poorly scattered silica nanoparticles are assembled at the interface to form clusters with several hundred nanometers in size (**Fig. S6b**).

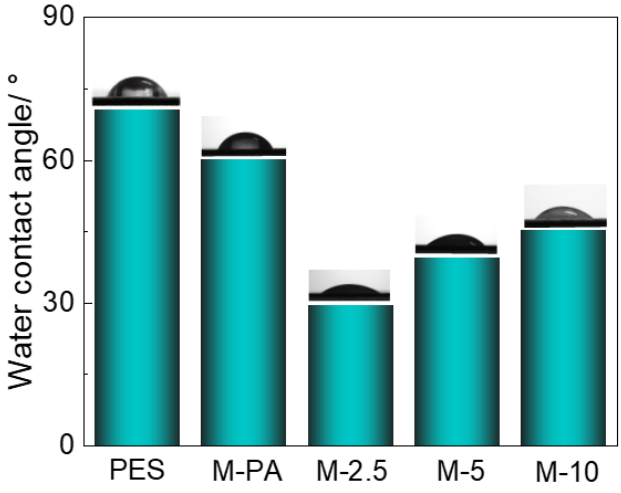

Fig. 6 Water contact angle (CA) of PES, **M-PA,** and **M-2.5**, **M-5**, **M-10**.

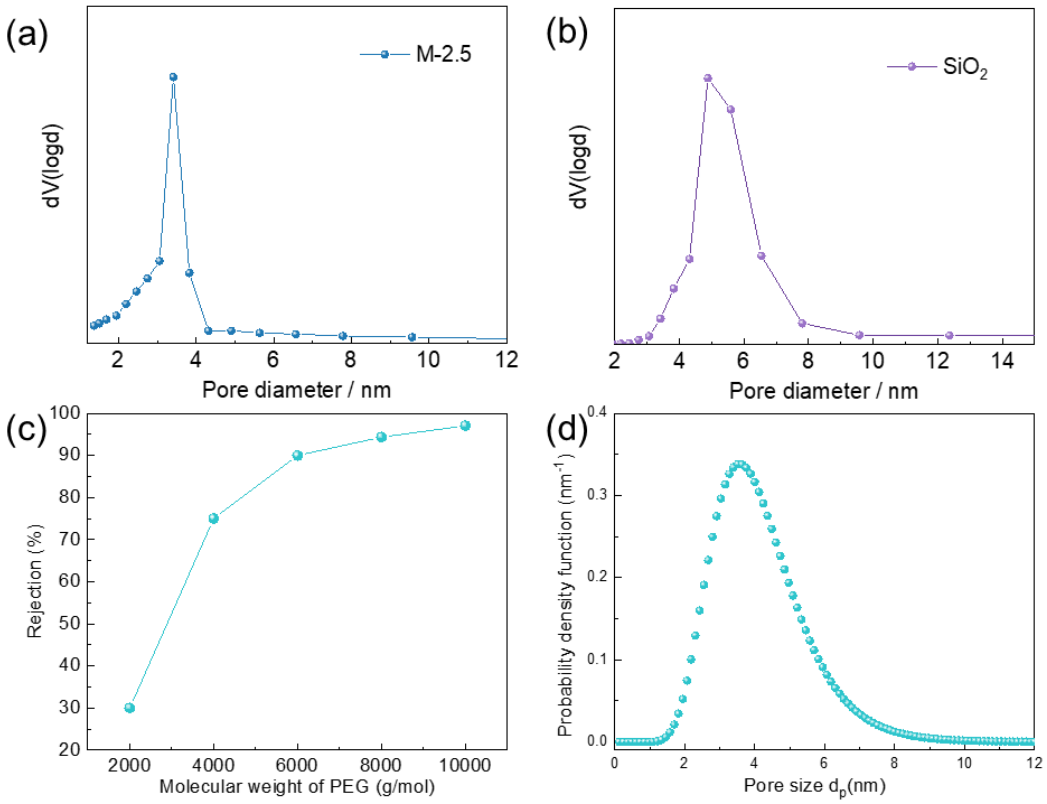

Fig. 7 Pore size distribution of **M-2.5** (a) and SiO_2 nanoparticles (b) according to N_2 adsorption isothermal curves; (c) Rejection curve of PEG with various molecular weights on the **M-2.5** membrane; (d) the probability density function and rejection curve-based calculation of the pore size distribution.

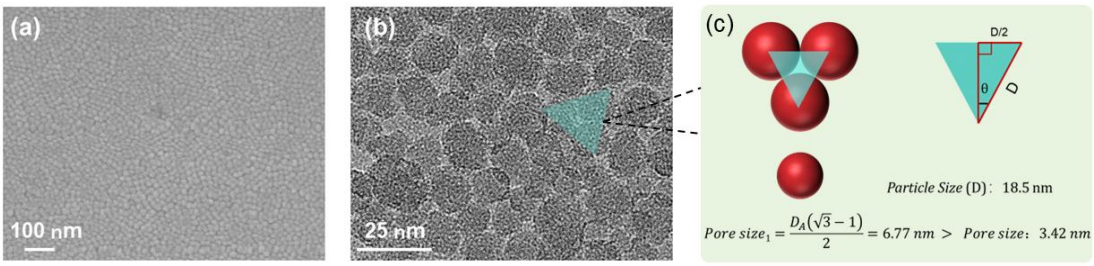

Fig. 8 SEM image (a) and TEM image (b) of regularly arranged SiO_2 nanoparticles in the flexible silica membranes; (c) the computed pore size distribution using a particle packing model.

3.3 The surface properties and pore size of flexible silica membrane

The hydrophilicity of **M-2.5** is assessed by the water contact angle (CA). As shown in **Fig. 6**, the CA of **M-2.5** is reduced from 60.17° to 29.60° in comparison with **M-PA**. It can impute to the presence of silanol groups (Si-OH) on SiO_2, which enhances the hydrophilicity of the flexible silica membranes. In addition, as the roughness

decreased, the CA increased from 29.6° (**M-2.5**) to 45.2° (**M-10**). Since the wettability of the solid substance is proportional to the roughness of the surface being wetted [35]. The surface charge properties of **M-2.5** is detected by zeta potential. As depicted in **Fig. S7**, the zeta potential gradually decreases with the increase in pH, which is caused by the adsorption and dissociation of protons from the silica surface groups (Si-OH). Besides, the isoelectric point (IEP) of **M-2.5** occurs at pH~3.0, and the surface of the membrane is strongly negatively charged (~ -50 mV) when the pH is approximately neutral, which facilitates efficient screening of negative dyes through electrostatic repulsion effect.

We have applied three different methods to evaluate the pore size of flexible silica membranes. (1) The average pore size of the flexible silica membrane was calculated according to N_2 adsorption isothermal curves (**Fig. S8**). As shown in **Fig. 7a**, the interfacial assembled flexible silica membrane exhibited a uniform pore size of 3.4 nm, which results from the uniform and close packing of the silica nanoparticles (**Fig. S6a**). In contrast, the intergranular voids have a wide distribution from 4 to 8 nm (**Fig. 7b**) due to the disordered and loosely packing of silica nanoparticles **(Fig. S6b**). (2) The pore size of the flexible silica membrane was also evaluated according to its rejection for PEGs. As illustrated in **Fig. 7c-d**, a log-normal model of pore size distribution is created using the rejection curve and a probability density function between rejection and Stokes radius. It reveals that the pore size of the flexible silica membrane is 3.6 nm, which is consistent with the results obtained from the N_2 adsorption. (3) The pore size of flexible silica membranes can also be estimated by mathematical models. According to the measurement results of the nanoparticle size analyzer, the average particle size of silica is 18.5 nm, and the minimum particle size is about 6.34 nm (**Fig. S2**). Assuming that silica nanoparticles are rigid balls and arranged regularly **(Fig. 8**), the calculated theoretical pore size distribution is 6.77 nm by the formulas of trigonometric functions, which is larger than the results obtained from the N_2 adsorption (3.4 nm) and measurement data of PEG (3.6 nm). The reason for the narrowing of the pore size of the silica layer is as follows: (1) The filling effect of small-sized silica nanoparticles (6.34 nm) for the pores packed by the large particles (18.5 nm). (2) The cross-linking effect of TMC tightly connects the adjacent silica nanoparticles. The shrinking pore size facilitates the effective separation of dyes.

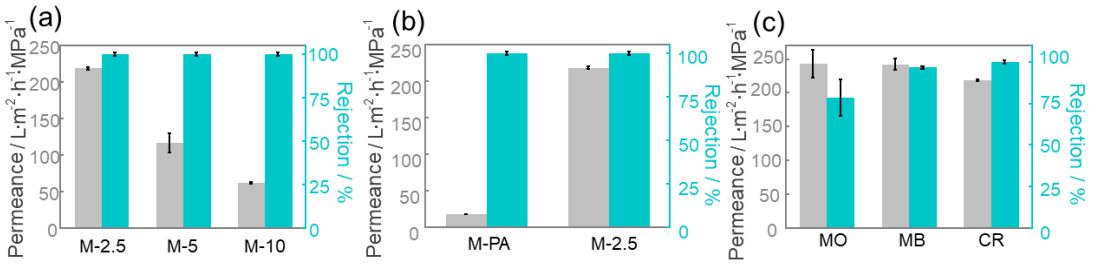

Fig. 9 (a) Influence of interfacial assembly time on flexible silica membranes separation performance, (b) CR dye separation properties of **M-2.5** and **M-PA**, (c) comparison of separation performance of **M-2.5** for different dyes. The permeance refers to Congo red solution.

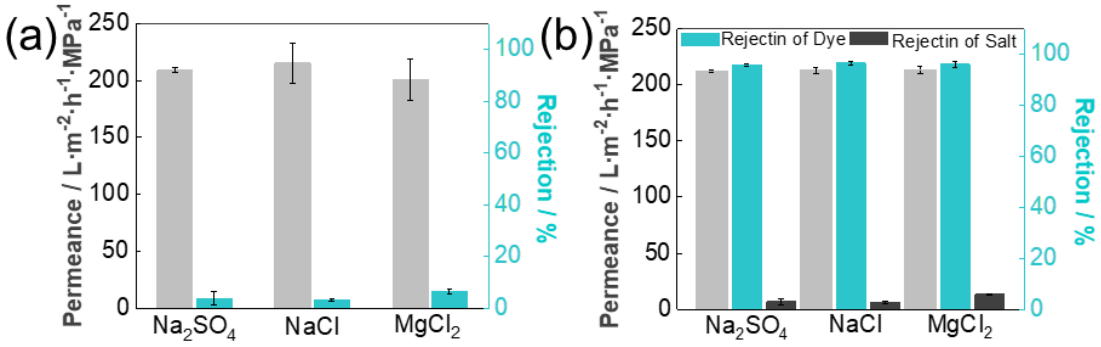

Fig. 10 (a) The NF performance for salt solutions (1000 ppm) on **M-2.5**, the permeance refers to Congo red solution; (b) NF performance of the **M-2.5** towards CR/salt mixed aqueous solution. Operate pressure: 0.2 MPa; CR and salt concentration: 50 ppm and 1000 ppm.

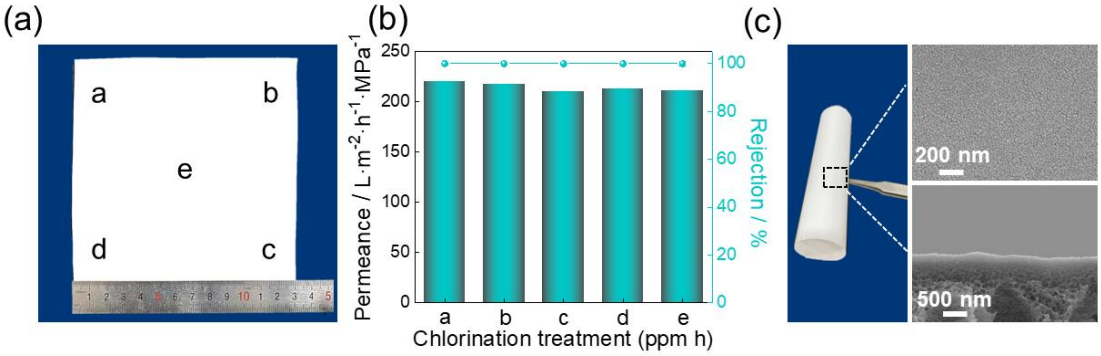

Fig. 11 (a) The **M-2.5** with a large area of 100 square centimeters; (b) the separation performance for CR of regions a-e in (a); (c) bending resistance test of **M-2.5**. The permeance refers to Congo red solution.

3.4 Separation performance of flexible silica membrane

Encouraged by the successful preparation of flexible silica membranes, the dye nanofiltration performance was estimated using a dead-end unit under 0.2 MPa. The effect of interfacial assembly time (2.5 to 10 mins) on the separation performance is shown in **Fig. 9a**. As the lengthening interface assembly time, the water permeance of flexible silica membranes is reduced from 218.68 (**M-2.5**) to 61.78 (**M-10**) L m^{-2} h^{-1} MPa^{-1}, due to the decrease of membrane hydrophilicity and the increase of membrane thickness. In addition, three flexible membranes exhibited nearly 100 % rejection of CR. It is demonstrated that a continuous and defect-free flexible silica membrane can be prepared in a short time (2.5 mins) by the interfacial assembly of SiO_2 nanoparticles.

The NF properties of **M-PA** and flexible silica membranes were compared using CR feed solution (50 ppm), and the results are shown in **Fig. 9b.** In comparison with the **M-PA** membrane, **M-2.5** shows enhanced water permeance from 18.37 to 218.68 L m^{-2} h^{-1} MPa^{-1} without the sacrifice of rejection (99.99 %). The better surface hydrophilicity of flexible silica membranes and the uniform accumulation pores (3.4 nm) facilitates the rapid transport of H_2O molecules while hindering large dye molecules, which boosts the performance of flexible silica membranes.

Three different dyes with varieties of sizes (MB, MO, and CR in **Table S1**) have been used to determine the main separation mechanism of the membrane. From **Fig. 9c,** it can be seen that **M-2.5** has the highest rejection for CR (~100 %), while the rejection for MB (96.65 %) and MO (78.53 %) decreases gradually. It indicates that the flexible silica membrane has a synergistic sieving mechanism with electrostatic repulsion as the primary effect and size sieving as the complementary effect. The rejection of negatively charged dyes with small sizes (MB, MO) relies mainly on the electrostatic repulsion effect between the negatively charged dye and the membrane surface (**Fig. S7**). As the size of the dye gradually increases, the size-sieving effect begins to emerge, thus achieving nearly complete rejection of CR dye. The **M-2.5** was also used to sieve ionic salt solutions (NaCl, Na_2SO_4, and $MgCl_2$). As depicted in **Fig. 10a**, the **M-2.5** membrane exhibits extremely low rejection for both monovalent and divalent salt solutions (6.55 % for $MgCl_2$, 3.90 % for Na_2SO_4, 3.45 % for NaCl), as the sizes of the hydrated ions are much smaller than the aperture of the membrane (ca. 3.4 nm). The filtration results of dye and ions indicate the potential use of flexible silica

membranes for the purification of dye sewage containing salts. Three different dye/salt mixtures including CR/NaCl, CR/Na_2SO_4, and CR/$MgCl_2$ were adopted to evaluate the dye/salt separation performance of **M-2.5**. It can be seen from **Fig. 10b** that when filtrated the mixture solutions, the rejection of the dye was slightly lower than the rejection measured by filtering a single dye solution (e.g., 99.99 % vs 96.50 % for CR), which may be due to the charge shielding effect of the salt[36, 37]. Nonetheless, **M-2.5** still possessed a relatively high rejection for CR (~96.50 %) and retained very low salt rejection (~2.65 % for NaCl, ~3.05 % for Na_2SO_4, ~5.90 % for $MgCl_2$). The appropriate pore size enables the rapid transport of ions and screen dye molecules effectively.

3.5 Scale-up preparation and stability of flexible silica membrane

To demonstrate the scalable production of **M-2.5**, the membrane with an area of 100 square centimeters was prepared through the interface assembly method in 2.5 mins (**Fig. 11a**). Five different regions (a-e in **Fig. 11a**) were selected for separation performance testing, achieving a rejection nearly 100 % for CR (**Fig. 11b**), which demonstrated that the enlarged membrane maintained excellent nanofiltration performance. The interface assembly method enables the scale-up preparation of inorganic membrane materials in a short time under room temperature. Meanwhile, the cross-linking effect of TMC between silica nanoparticles improves the flexibility of the membrane. As demonstrated in **Fig. 11c**, **M-2.5** has no morphological changes on the surface and section after the curvature of 100 m^{-1} is rolled, proving the overall flexibility of the membrane. The curvature of bending is the reciprocal of the radius (curvature $K = 1/r$).

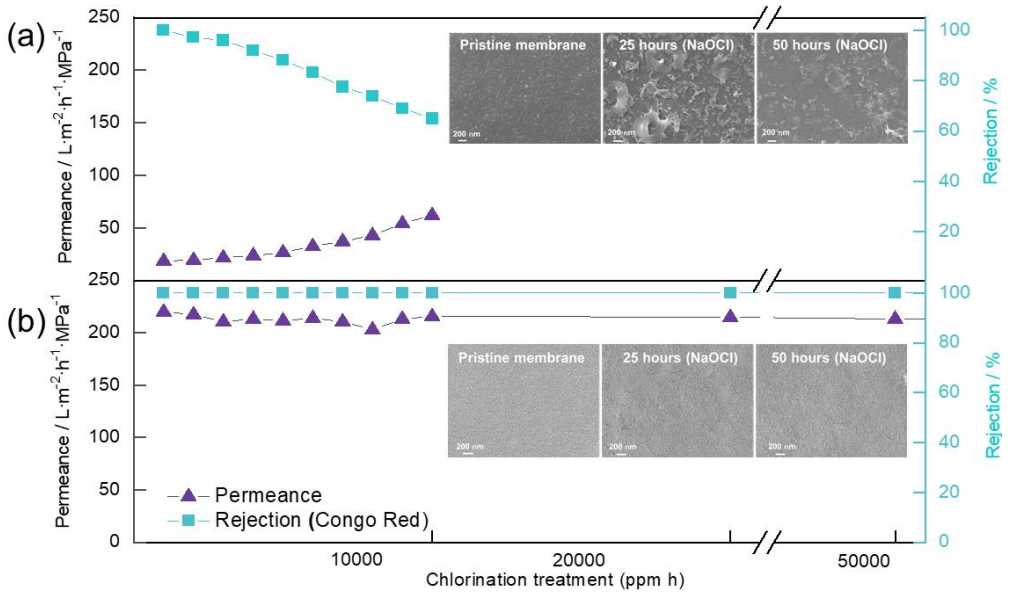

Fig. 12 Separation performance of (a) **M-PA** and (b) **M-2.5** exposed to 200 ppm NaOCl aqueous solution. The insert in (a) and (b) are the SEM images of the **M-PA** membrane and **M-2.5** membrane after immersion in 200 ppm NaOCl solution for 0 hours, 25 hours, and 50 hours. The permeance refers to Congo red solution.

Table 2. NF performance of **M-2.5** and other reference membranes

Membrane	Dye	Chlorine resistance	Permeance ($L\ m^{-2}\ h^{-1}MPa^{-1}$)	Rejection (%)	Ref.
Flexible silica membrane	**Methyl blue Congo red**	**50000 ppm h**	**218.68**	**96.74 % 99.99 %**	**This work**
M-PA	Congo red	Poor	18.04	99.99 %	
TEPA/TMC	Orange GII	14400 ppm h	150	90 %	[38]
DST/TMC	Rose Bengal	24000 ppm h	152.7	98.26 %	[39]
GO	Congo red	-	82	98.97%	[40]
rGO	Congo red	-	160	99 %	[41]
PA/Fe-Cage	Congo red	Poor	52.66	96 %	[42]
PA/ZIF-8	RB_2	Poor	149	99.2 %	[43]
PA-EDC-BS4	Congo red	Poor	125	99.8 %	[44]

Unlike traditional amide structures, flexible silica membranes based on ester linkages exhibit improved chlorine resistance. The chlorine resistance of the **M-PA** and flexible silica membrane were compared through the active chlorine immersion method. As anticipated, the permeance of the **M-PA** began to gradually increase after soaking in an active chlorine solution (200 ppm) for 5 hours, while the rejection of CR gradually decreased, which should be due to the deterioration of the polyamide active layer proved by SEM (**Fig.12a**). In contrast, the flexible silica membrane (**M-2.5**) maintains its uniform and smooth surface topography after immersing in the active chlorine solution for 50 hours (**Fig. 12b)**. The rejection for CR after a total free chlorine exposure of 50000 ppm h (200 ppm for 250 hours) was maintained, suggesting the potential of **M-2.5** for treating chlorine-rich water. Long-term stability (250 hours) of the water permeance and dye rejection also proves the sieving effect of the silica layer rather than adsorption. Because the adsorption-induced separation effect will be gradually weakened after reaching the adsorption saturation point. The pure water flux at various pressures was evaluated to verify the strong structural

stability of the membrane. As observed in **Fig. S9**, the water flux of **M-2.5** rose linearly with pressure in the range of 0.2 to 1 MPa. The structural stability of silica nanoparticles is conducive to maintaining the NF performance of the membrane under high pressure.

In contrast with other reported NF membranes, the membrane demonstrated superior NF performance (**Table 2**). It is noticeable that the flexible silica membrane has higher water permeance than traditional TFC membranes (MPD/TMC, TEPA/TMC, DST/TMC), GO membranes, and thin-film nanocomposite (TFN) membranes (PA/Fe-Cage, PA/ZIF-8, and PA-EDC-BS4). In addition, the membrane can maintain excellent dye separation performance under the long-term high concentration of active chlorine, showing high stability.

4. Conclusion

In summary, the facile interfacial assembly method was adopted to prepare a flexible silica membrane. The ultra-small sized silica nanoparticles and highly reactive TMC were selected as the water monomers and the oil monomers respectively. Through precise control of reactant concentration and dispersion state, a continuous flexible silica membrane was obtained on the PES substrate. The flexible PES substrate and the cross-linking effect of TMC endow the membrane with good flexibility, which could keep the structure after bending to 100 m^{-1} curvature. Due to the uniform pore size (3.4 nm) and excellent hydrophilicity of the membrane as well as negative surface zeta potential, the water permeance of the flexible silica membrane exceeds 210 L m^{-2} h^{-1} MPa^{-1}, which was enhanced by 1112.2 % from the **M-PA** membrane, simultaneously with a 99.99 % dye rejection. Meanwhile, the cross-linking structure based on ester bonds guarantees the membrane excellent chlorine resistance, the membrane can maintain its separation performance after being immersed in active chlorine at 200 ppm for 250 hours. The results show that the interfacial assembly strategy may be an alternative method to fabricate flexible inorganic membranes.

Acknowledgments

This work was supported by the National Key Research and Development Program of China of Ministry of Science and Technology (2022YFE0116000), National Natural Science Foundation of China (No. 22175200, No. 21975285, No. 22171288), Fujian

Province Science and Technology Program, Innovation Fund (2022C0021), Shandong Province Natural Science Foundation (ZR2020MB017), and the Outstanding Youth Science Fund Projects of Shandong Province (ZR2022YQ15).

References

[1] M. Cheryan, N. Rajagopalan, Membrane processing of oily streams. Wastewater treatment and waste reduction, J. Membr. Sci. 151 (1998) 13–28.

[2] C.-Z. Liang, S.-P. Sun, F.-Y. Li, Y.-K. Ong, T.-S. Chung, Treatment of highly concentrated wastewater containing multiple synthetic dyes by a combined process of coagulation/flocculation and nanofiltration, J. Membr. Sci. 469 (2014) 306-315.

[3] A.K. An, J. Guo, S. Jeong, E.-J. Lee, S.A.A. Tabatabai, T. Leiknes, High flux and antifouling properties of negatively charged membrane for dyeing wastewater treatment by membrane distillation, Water Res. 103 (2016) 362-371.

[4] M.C.M. van Loosdrecht, D. Brdjanovic, Anticipating the next century of wastewater treatment, Science. 344 (2014) 1452-1453.

[5] L. Yang, Z. Wang, J. Zhang, Zeolite imidazolate framework hybrid nanofiltration (NF) membranes with enhanced permselectivity for dye removal, J. Membr. Sci. 532 (2017) 76–86.

[6] Z. Aksu, E. Balibek, Effect of salinity on metal-complex dye biosorption by Rhizopus arrhizus, J. Environ. Manage. 91 (2010) 1546-1555.

[7] G.J.B.t. Crini, Non-conventional low-cost adsorbents for dye removal: a review, Bioresour. Technol. 97 (2006) 1061-1085.

[8] L. Wang, S. Ji, N. Wang, R. Zhang, J.R. Li, One-step self-assembly fabrication of amphiphilic hyperbranched polymer composite membrane from aqueous emulsion for dye desalination, J. Membr. Sci. 452 (2014) 143–151.

[9] M.A. Shannon, P.W. Bohn, M. Elimelech, J.G. Georgiadis, B.J. Mariñas, A.M. Mayes, Science and technology for water purification in the coming decades, Nature. 452 (2008) 301-310.

[10] B. Bolto, T. Tran, M. Hoang, Z.L. Xie, Crosslinked poly (vinyl alcohol) membranes, Prog. Polym. Sci. 34 (2009) 969-981.

[11] X. Jiang, S. Li, L. Shao, Pushing CO_2-philic membrane performance to the limit by designing semi-interpenetrating networks (SIPN) for sustainable CO_2 separations, Energy Environ. Sci. 10 (2017) 1339-1344.

[12] P. Marchetti, M.F. Jimenez Solomon, G. Szekely, A.G. Livingston, Molecular separation with organic solvent nanofiltration: a critical review, Chem. Rev. 114 (2014) 10735-10806.

[13] S. Karan, Z. Jiang, A.G. Livingston, Sub-10 nm polyamide nanofilms with ultrafast solvent transport for molecular separation, Science. 348 (2015) 1347-1351.

[14] X. Lu, M. Elimelech, Fabrication of desalination membranes by interfacial polymerization: history, current efforts, and future directions, Chem. Soc. Rev. 50 (2021) 6290-6307.

[15] Z. Tan, S. Chen, X. Peng, L. Zhang, C. Gao, Polyamide membranes with nanoscale Turing structures for water purification, Science. 360 (2018) 518-521.

[16] M.B. Wu, Y. Lv, H.C. Yang, L.F. Liu, X. Zhang, Z.K. Xu, Thin film composite membranes combining carbon nanotube intermediate layer and microfiltration support for high nanofiltration performances, J. Membr. Sci. 515 (2016) 238–244.

[17] V.T. Do, C.Y. Tang, M. Reinhard, J.O. Leckie, Effects of chlorine exposure conditions on physiochemical properties and performance of a polyamide membrane-mechanisms and implications, Environ. Sci. Technol. 46 (2012) 13184-13192.

[18] R.J.J.J.o.m.s. Petersen, Composite reverse osmosis and nanofiltration membranes, J. Membr. Sci. 83 (1993) 81-150.

[19] W. Lau, A. Ismail, N. Misdan, M.J.D. Kassim, A recent progress in thin film composite membrane: a review, Desalination. 287 (2012) 190-199.

[20] H. Fan, A. Mundstock, A. Feldhoff, A. Knebel, J. Gu, H. Meng, J. Caro, Covalent organic framework-covalent organic framework bilayer membranes for highly selective gas separation, J. Membr. Sci.140 (2018) 10094-10098.

[21] Y. Li, Q. Wu, X. Guo, M. Zhang, B. Chen, G. Wei, X. Li, X. Li, S. Li, L.-J. Ma, Laminated self-standing covalent organic framework membrane with uniformly distributed subnanopores for ionic and molecular sieving, Nat. Commun. 11 (2020) 1-9.

[22] X. Wang, C. Chi, K. Zhang, Y. Qian, K.M. Gupta, Z. Kang, J. Jiang, D. Zhao, Reversed thermo-switchable molecular sieving membranes composed of two-dimensional metal-organic nanosheets for gas separation, Nat. Commun. 8 (2017) 1-10.

[23] P.S. Goh, A.F. Ismail, A review on inorganic membranes for desalination and wastewater treatment, Desalination. 434 (2018) 60-80.

[24] T.J.S. Tsuru, p. methods, Inorganic porous membranes for liquid phase separation, Sep. Purif. Methods. 30 (2001) 191-220.

[25] A. Larbot, S. Alami-Younssi, M. Persin, J. Sarrazin, L. Cot, Preparation of a γ-alumina nanofiltration membrane, J. Membr. Sci. 97 (1994) 167-173.

[26] S. Qiu, M. Xue, G. Zhu, Metal-organic framework membranes: from synthesis to separation application, Chem. Soc. Rev. 43 (2014) 6116-6140.

[27] A. Huang, W. Dou, J. Caro, Steam-stable zeolitic imidazolate framework ZIF-90 membrane with hydrogen selectivity through covalent functionalization, J. Am. Chem. Soc. 132 (2010) 15562-15564.

[28] A. Huang, H. Bux, F. Steinbach, J. Caro, Molecular- sieve membrane with hydrogen permselectivity: ZIF- 22 in LTA topology prepared with 3- aminopropyltriethoxysilane as covalent linker, Angew. Chem., Int. Ed. Engl. 122 (2010) 5078-5081.

[29] H. Guo, Y. Zhu, S. Qiu, J.A. Lercher, H.J.A.M. Zhang, Coordination modulation induced synthesis of nanoscale Eu1- xTbx- metal- organic frameworks for luminescent thin films, Adv. Mater. 22 (2010) 4190-4192.

[30] F. Zhang, X. Zou, X. Gao, S. Fan, F. Sun, H. Ren, G.J.A.F.M. Zhu, Hydrogen selective NH_2- MIL- 53 (Al) MOF membranes with high permeability, Adv. Funct. Mater. 22 (2012) 3583-3590.

[31] C.Y. Tang, Y.-N. Kwon, J.O. Leckie, Effect of membrane chemistry and coating layer on physiochemical properties of thin film composite polyamide RO and NF membranes: I. FTIR and XPS characterization of polyamide and coating layer chemistry, Desalination. 242 (2009) 149-167.

[32] J. Lin, W. Ye, M.-C. Baltaru, Y.P. Tang, N.J. Bernstein, P. Gao, S. Balta, M. Vlad, A. Volodin, A. Sotto, P. Luis, A.L. Zydney, B. Van der Bruggen, Tight ultrafiltration membranes for enhanced separation of dyes and Na_2SO_4 during textile wastewater treatment, J. Membr. Sci. 514 (2016) 217-228.

[33] J.-P. Gallas, J.-M. Goupil, A. Vimont, J.-C. Lavalley, B. Gil, J.-P. Gilson, O.J.L. Miserque, Quantification of water and silanol species on various silicas by coupling IR spectroscopy and in-situ thermogravimetry, Langmuir. 25 (2009) 5825-5834.

[34] M. Jayarani, S.J.D. Kulkarni, Thin-film composite poly (esteramide)-based membranes, Desalination. 130 (2000) 17-30.

[35] R.N.J.I. Wenzel, E. Chemistry, Resistance of solid surfaces to wetting by water, Ind. Eng. Chem. 28 (1936) 988-994.

[36] F.-Y. Zhao, Y.-L. Ji, X.-D. Weng, Y.-F. Mi, C.-C. Ye, Q.-F. An, C.-J. Gao, High-flux positively charged nanocomposite nanofiltration membranes filled with poly (dopamine) modified multiwall carbon nanotubes, ACS Appl. Mater. Interfaces. 8 (2016) 6693-6700.

[37] M. Peydayesh, T. Mohammadi, O.J.S. Bakhtiari, P. Technology, Effective treatment of dye wastewater via positively charged TETA-MWCNT/PES hybrid nanofiltration membranes, Sep. Purif. Technol. 194 (2018) 488-502.

[38] X. Fan, Y. Dong, Y. Su, X. Zhao, Y. Li, J. Liu, Z.-Y. Jiang, Improved performance of composite nanofiltration membranes by adding calcium chloride in aqueous phase during interfacial polymerization process, J. Membr. Sci. 452 (2014) 90-96.

[39] M.B.M.Y. Ang, G.-W. Huang, M.-Y. Chu, J.C. Millare, S.-H. Huang, K.-R.J.J.o.W.P.E. Lee, Use of aqueous polyol monomer for superior dye separation performance and high chlorine resistance of thin-film composite polyester nanofiltration membranes, J. Water. Process. Eng. 48 (2022) 102843.

[40] J. Wang, P. Zhang, B. Liang, Y. Liu, T. Xu, L. Wang, B. Cao, K. Pan, Graphene oxide as an effective barrier on a porous nanofibrous membrane for water treatment, ACS Appl. Mater. Interfaces, 8 (2016) 6211-6218.

[41] X. Fan, C. Cai, J. Gao, X. Han, J. Li, Hydrothermal reduced graphene oxide membranes for dyes removing, Sep. Purif. Technol, 241 (2020) 116730.

[42] C. Zhang, X. Si, S. Zhang, B. Pei, J. Gu, Y.-X. Bai, Porous metal–organic molecular cage: a promising candidate to highly improve the nanofiltration performance of thin film nanocomposite membranes, New J. Chem, 43 (2019) 1699-1709.

[43] J. Zhu, L. Qin, A. Uliana, J. Hou, J. Wang, Y. Zhang, X. Li, S. Yuan, J. Li, M.J.A.a.m. Tian, interfaces, Elevated performance of thin film nanocomposite membranes enabled by modified hydrophilic MOFs for nanofiltration, ACS Appl. Mater. Interfaces. 9 (2017) 1975-1986.

[44] M. Liu, Q. He, K. Zhang, Z. Guo, Z. Lü, S. Yu, C.J.J.o.h.m. Gao, Carbodiimide-assisted zwitterionic modification of poly (piperazine amide) thin-film composite membrane for enhanced separation and anti-depositing performances to cationic/anionic dye aqueous solutions, J. Hazard Mater. 396 (2020) 122582.